Colloidal Photonic Crystals with Narrow Stopbands Assembled from Low-Adhesive Superhydrophobic Substrates

Yu Huang,[†,‡,⊥] Jinming Zhou,[†,‡,⊥] Bin Su,[†,‡] Lei Shi,[§] Jingxia Wang,[*,†] Shuoran Chen,[†,‡] Libin Wang,[†,‡] Jian Zi,[§] Yanlin Song,[*,†] and Lei Jiang[†]

[†]Beijing National Laboratory for Molecular Sciences (BNLMS), Laboratory of New Materials, Key Laboratory of Organic Solids, Institute of Chemistry, Chinese Academy of Sciences, Beijing 100190, P.R. China

[‡]Graduate University of Chinese Academy of Sciences, Beijing 100049, P.R. China

[§]Department of Physics and Key Laboratory of Micro and Nano Photonic Structures (Ministry of Education), Fudan University, Shanghai 200433, P.R. China

Ⓢ Supporting Information

ABSTRACT: This article presents a facile approach to centimeter-scale colloidal photonic crystals (PCs) with narrow stopbands assembled on low-adhesive superhydrophobic substrates. The full-width-at-half-maxima of the stopbands are just 12 nm. The narrow stopbands of colloidal PCs are ascribed to the combined effects of perfectly ordered assembly structure, large-scale crack elimination, decreased void fraction, and sufficient thickness of the colloidal PCs. These properties result from a self-assembly process on a low-adhesive superhydrophobic substrate. Latex suspension on this substrate displays a receding three-phase contact line during evaporation, which releases tensile stress induced by latex shrinkage and results in complete elimination of cracks in the colloidal PCs. Furthermore, the simultaneous assembly of latex particles on the outermost layer of a spread liquid film contributes to the perfectly ordered assembly structure. This facile fabrication of centimeter-scale colloidal PCs with narrow stopbands will offer significant insights into the design and creation of novel optical devices.
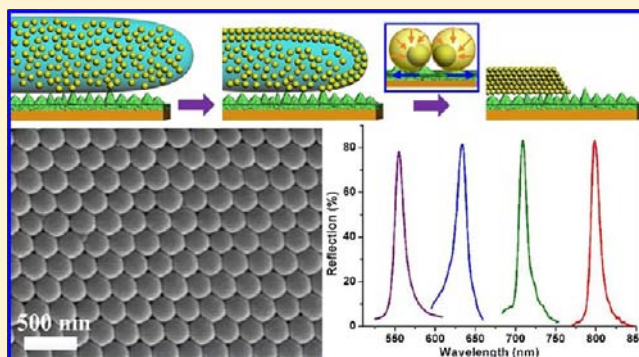
INTRODUCTION

Three-dimensional periodic dielectric materials theoretically demonstrate the ability to possess a photonic band gap (PBG).[1] Such PBG materials, commonly known as photonic crystals (PCs), are of interest in the emerging area of optical materials for controlling and manipulating light propagation[2] and have shown promising applications in catalyst,[3] sensing,[4] label-free detection,[5] high-performance optical devices,[6] and other fields.[7] Various novel materials and assembly structures have been developed for improving the optical qualities of colloidal PCs and achieving special optical signals for the extensive applications of PC-based optical devices.[8−12] Examples include adopting high refractive index materials such as Si or Ge to achieve complete PBG PCs,[8] employing a two-dimensional particle array to achieve ultrahigh diffraction for sensing,[9] transforming bioinspired structures for angle-independent reflection bands or full-color pixels,[10] or exploiting nonspherical building blocks for PCs with special optical properties.[11] However, it is still a challenge to fabricate large-scale PCs with narrow stopbands, due to the difficulty in achieving PCs with combined properties of homogeneously well-ordered latex assembly, large-area crack elimination, decreased void fraction, and sufficient thickness. This is of special importance for

improving the resolution and sensitivity of PC-based devices and the extension of PCs' applications to various advanced optical filters.[13] Here, we put forward a facile strategy for the fabrication of colloidal PCs with narrow stopbands from low-adhesive superhydrophobic substrates.

Adhesive interaction between latex suspension and substrate plays a crucial role in the assembly structures, owing to their significant effect on the production of tensile stress and crack formation during the assembly process.[14,15] Recently, researchers revealed improved assembly structure[9,16−19] from hydrophilic[16a−c] or liquid interfaces[9,17−19] with distinct surface tensions and adhesive forces (F_{ad}). Typical examples include simultaneous supracrystal growth of gold PCs at the air–toluene interface,[17a] homogeneous orientation of anisotropic particles at the air–water interface,[17b,c] and high-reflectivity assembly structures on Hg surfaces.[9] Here, we demonstrate colloidal PCs with a narrow full-width-at-half-maxima (FWHM) stopband approaching 12 nm from low-adhesive superhydrophobic substrates. The narrow stopband could be attributed to the combined effects of perfectly ordered assembly

structure, large-scale crack elimination, decreased void fraction, and sufficient thickness of the resultant colloidal PCs. These properties profit from the low-adhesive superhydrophobic substrate. The latex suspension on this substrate is in the Cassie regime and undergoes an obvious receding of solid−liquid−gas three-phase contact line (TCL) during the drying process. The receding of TCL causes a timely release of the stress induced from latex shrinkage, leading to complete crack elimination and a more close-packed assembly structure. Furthermore, the simultaneous nucleation and crystallization of latex particles on the outermost layer of spreading liquid film produce a perfect assembly structure spanning whole PCs. This facile fabrication of colloidal PCs with narrow stopbands will be of great importance not only for the development of PC-based optical devices but also for the extensive creation of various advanced crystal structures of other materials.

■ RESULTS AND DISCUSSION

Figure 1 displays scanning electron microscope (SEM) images of the PCs assembled from latex particles with diameters of 224
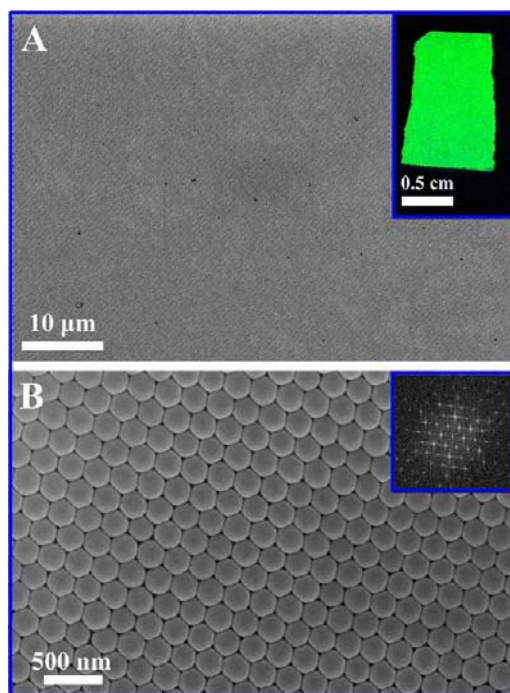
Figure 1. SEM images of the as-prepared colloidal PCs with diameter of 224 nm assembled on low-adhesive superhydrophobic substrate. Inset in (A) is a photograph of a part of the PCs, with the scale bar of 0.5 cm. Inset in (B) is a Fourier format (FFT) image obtained from a large-area SEM image. The images demonstrate perfectly ordered latex arrangement and close-packed assembly structures of the PCs.

nm on a low-adhesive superhydrophobic substrate. The monodisperse latex particles have polystyrene cores and poly(methyl methacrylate)−poly(acrylic acid) shell.[20] The polydispersity index of latex particles is lower than 0.006 (Figure S5, Supporting Information [SI]), which contributes to a perfectly ordered latex arrangement. The perfectly ordered latex arrangement can be seen at the (111) face of the face-centered cubic structure, spanning dozens of micrometers with few defects and line dislocations, and large-scale crack elimination. The FFT image in the inset of Figure 1B and the atomic force microscope (AFM) image in Figure 2A also
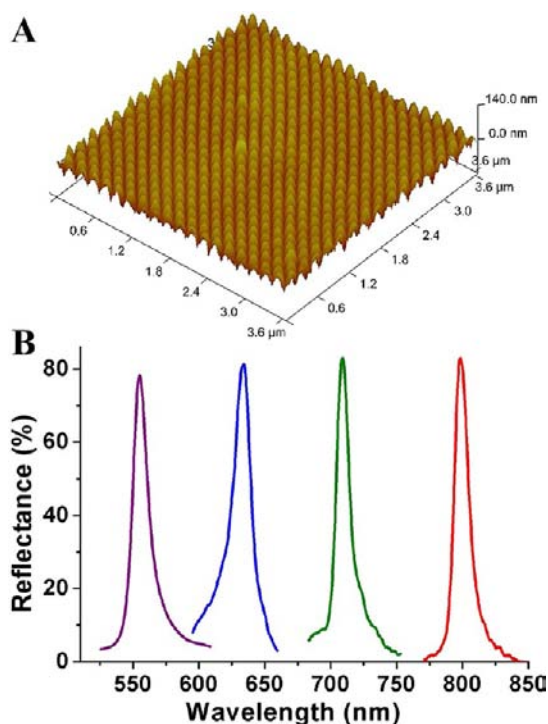

Figure 2. Typical AFM image (A), and UV−vis reflection spectra of colloidal PCs from latex particles with various diameters (B) assembled on the low-adhesive superhydrophobic substrates. The stopband positions are 555, 635, 708, and 796 nm for PCs assembled from latex particles with respective diameters of 224, 258, 286, and 320 nm and with respective FWHMs of the stopbands of 12, 15, 12, and 12 nm, respectively.

demonstrate perfectly ordered latex arrangement and close-packed assembly structures of the PCs. It should be noted that the latex particles are arranged in a more close-packed way, i.e. "area contact pattern" among latex particles. This is different from the traditional "point contact pattern" of common assembly structures.[21] This close-packed pattern results from the special structure of the latex particles. The soft PAA latex shell is prone to deform on low-adhesive, superhydrophobic substrates, as shown in Figure 1B. Both the close-packed assembly structure and the large-scale crack elimination contribute to the high optical properties in Figure 2B. Their stopband positions are 555, 635, 708, and 796 nm, respectively, for PCs assembled from latex particles with diameters of 224, 258, 286, and 320 nm. All the intensities of their stop bands exceed 80%, and their FWHMs are 12, 15, 12, and 12 nm, respectively.

To clarify the factors contributing to the well-ordered latex assembly and narrow stopbands of the colloidal PCs, we investigated the influence of substrates with different F_{ad} on the morphologies and optical properties of as-prepared colloidal PCs. The substrates with different adhesive behaviors were prepared by coating the polydimethylsiloxane (PDMS)-modified silica nanoparticles solution (in chloroform) with different concentrations.[22] The morphology of the as-prepared substrates can be effectively modified as shown in Figure 3. A gradual increment of the surface roughness can be achieved on the substrates when increasing the concentration of silica nanoparticles in the coating solution. The roughness (R_a) of the substrates grows from 1.78 ± 0.53, 3.74 ± 0.22, 4.26 ± 0.47, 5.68 ± 0.37, to 5.94 ± 0.34 μm, when the silica nanoparticles
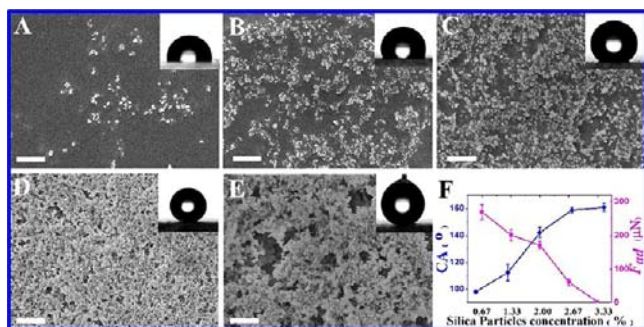
Figure 3. SEM images of the substrates with different F_{ad} and photographs of a water droplet on the corresponding surfaces (insets): 269 ± 25 μN, with CA of $98.2 \pm 1.2°$ (A), 201 ± 19 μN, with CA of $112.4 \pm 6.1°$ (B), 171 ± 16 μN, with CA of $142.1 \pm 3.8°$ (C), 60 ± 7 μN, with CA of $158.7 \pm 1.9°$ (D), and 2 ± 1 μN, with CA of $160.8 \pm 3.2°$ (E). The scale bars are 500 nm. (F) Relationship between the CA/F_{ad} of the treated substrates and the concentrations of the used silica nanoparticle solutions. The roughness (R_a) of the substrates is 1.78 ± 0.53 μm (A), 3.74 ± 0.22 μm (B), 4.26 ± 0.47 μm (C), 5.68 ± 0.37 μm (D), and 5.94 ± 0.34 μm (E), characterized by Surtronic 25, Taylor Hobson precision (England).

concentration is increased from 0.6%, 1.3%, 2.0%, and 2.6% to 3.3%. With the rise of the roughness, there is an obvious increase of water contact angle (CA) and decrease of F_{ad}. When the water CAs of the substrates increase from $98.2 \pm 1.2°$, $112.4 \pm 6.1°$, $142.1 \pm 3.8°$, and $158.7 \pm 1.9°$ to $160.8 \pm 3.2°$, the F_{ad} values of the corresponding substrates lower from 269 ± 25, 201 ± 19, 171 ± 16, and 60 ± 7 to 2 ± 1 μN, respectively.

Figure 4 shows the typical water adhesive behavior on different substrates. The water droplet attaches to the substrate
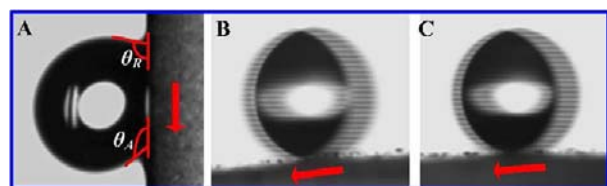

Figure 4. Sliding behavior of a water droplet on the substrates with various F_{ad}. No droplet rolls even when the substrate (with F_{ad} of 269 ± 25 μN) is tilted to 90° (A). Droplet rolls when the substrate (with F_{ad} of 60 ± 7 μN) is tilted just 6° (B) and when the substrate (with F_{ad} of 2 ± 1 μN) is tilted less than 3° (C). The arrows show the roll direction of the water droplet. The substrates with different F_{ad} show distinct adhesive behaviors for a water droplet upon it.

with F_{ad} of 269 ± 25 μN (Figure 4A), even if the substrate is tilted at 90°. In this case, the CA is larger at the bottom (advancing angle, θ_A) than that at the top (receding angle, θ_R), which implies high CA hysteresis and suggests that the contact mode of the water droplet on this substrate is in the Wenzel regime.[23] In contrast, the water droplets easily roll away from substrates with F_{ad} of 60 ± 7 μN and 2 ± 1 μN when the substrates are only slightly titled. For example, 6° tilting is required for a water droplet rolling away from the substrate with F_{ad} of 60 ± 7 μN (Figure 4B), and less than 3° for tilting on substrate with F_{ad} of 2 ± 1 μN (Figure 4C). The phenomena indicates the water droplet on substrate with F_{ad} lower than 60 ± 7 μN is in the Cassie regime and displays low water adhesion properties.[24] The distinct adhesive behaviors of

the substrates are critical for the latex particles' assembly and the optical property of the PCs.

Figure 5 presents reflectance spectra of PCs assembled on substrates with different F_{ad}. Obvious red-shift and narrowing
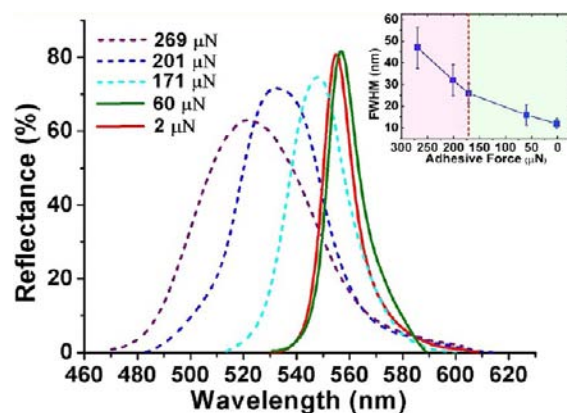
Figure 5. Reflectance spectra of PCs assembled on substrates with different F_{ad}. The inset indicates the relationship between the FWHM of PCs and the F_{ad} of the corresponding substrates. The red- or green-shaded region indicates cracked or crack-free PCs, respectively. Obvious red-shift and narrowing (inset) are found for the stopbands of as-prepared PCs with decreased F_{ad} of the substrates. FWHM of PCs changes from 47, 32, 26, and 16, to 12 nm when the F_{ad} drops from 269 ± 25, 201 ± 19, 171 ± 16, and 60 ± 7 to 2 ± 1 μN.

(inset) are found for the stopbands of as-prepared PCs with decreased F_{ad} of the substrates. It is notable that a significant reduction of cracks for the PCs assembled on the substrate with F_{ad} less than ~171 μN, as indicated in inset graph of Figure 5. This phenomenon implies a critical condition for large-scale crack elimination. To estimate this critical value, the theoretical critical force for crack formation is calculated using Griffith's energy balance concept.[14] The theoretical value is 156 μN, very close to the experimental value of 171 μN. This implies the force of restricting latex shrinkage is insufficient to induce cracking when the F_{ad} of the substrate is lower than 156 μN (Figure S6, SI). The FWHMs decrease from 47, 32, 26, and 16, to 12 nm, and the stopband peaks move from 776 to 798 nm when F_{ad} values of assembled substrates drop from 269 ± 25, 201 ± 19, 171 ± 16, and 60 ± 7 to 2 ± 1 μN. The red-shift of the peak positions of PCs (Figure 5) can be explained by Bragg's law:[25]

$$\lambda_{max} = 2d_{111}n_{eff}\sin\theta$$

$$n_{eff}^2 = fn_0^2 + (1-f)n_c^2$$

$$d_{111} = \sqrt{2/3}\,D$$

where λ_{max} is the maximum wavelength of reflectance; d_{111} is the lattice spacing, which is equal to $((2/3)^{1/2})D$; n_{eff} is the effective refractive index of the colloidal PCs; $n_c = 1$ and $n_0 = 1.60$ are the refractive index of the air and the polystyrene respectively; D is the diameter of the latex particles; θ is an angle of incidence, and $\theta = 90°$ in our experiment; f is the filling factor of the as-prepared colloidal PCs, which is determined by assembly structure of latex particles. The large-scale crack elimination and more close-packed structure of PCs will make the value of f grow.
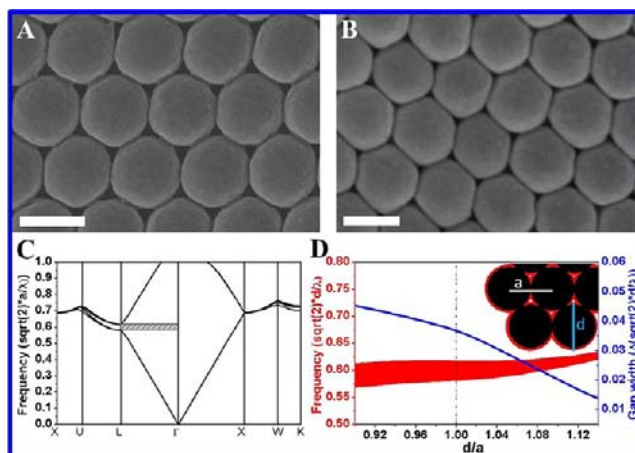
In detailed, obvious cracks could be found in A and B of Figure 6 for colloidal PCs assembled on high-adhesive
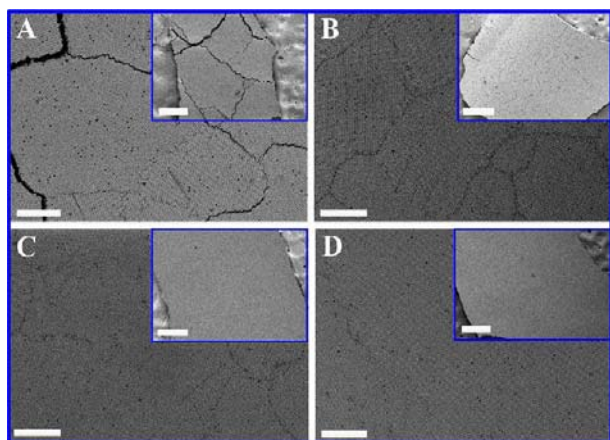
Figure 6. SEM images of colloidal PCs assembled on substrates with varying F_{ad}. The F_{ad} decreases from 269 ± 25 μN (A), 201 ± 19 μN (B), 171 ± 16 μN (C) to 2 ± 1 μN (D). The scale bars are 10 μm, and that in insets are 0.5 mm. These SEM images indicate that cracks are eliminated in large scale for the colloidal PCs assembled on substrate with F_{ad} lower than 171 ± 16 μN.

Figure 7. SEM images of PCs assembled on substrates with high F_{ad} (A) and low F_{ad} (B), displaying more close-packed assembly structure on low-adhesive superhydrophobic substrates. The photonic band structure of ideal colloidal PCs is calculated based on plane wave expansion (C), the band edge frequency (red region) and the gap (blue line) as a function of the ratio between the diameter and period (D). Inset in D is an explanation for d (particles' diameter) and a (center-to-center distance between two adjacent particles). As the assembly structure becomes denser, d/a increases, and the gap width decreases.

substrates ($F_{ad} > 201 \pm 19$ μN). When F_{ad} of substrate is lower than 171 ± 16 μN, the latex particles are perfectly assembled and without cracks in large-scale (C and D of Figure 6). It means the filling factor f is higher on substrates with low F_{ad} than that on substrates with high F_{ad}. As F_{ad} of the substrates decreases, the as-prepared PCs will have less cracks, thus f and n_{eff} become larger, and cause larger λ_{max}. Accordingly, an obvious red-shift of the stopband position is observed for colloidal PCs assembled on substrate with varying F_{ad} from 269 ± 25 to 2 ± 1 μN. It indicates that the large-scale crack elimination may play a more important role for the stopband position than the change of lattice interstice.

There are many factors contribute to the photonic band gap.[26] Here, we focus on the influence of particles assembly structures on substrates with various F_{ad}: point contact pattern from high-adhesive substrates and area contact pattern from low-adhesive superhydrophobic substrates. We calculated the photonic band structure, the relationship of the assembly structure with the frequency of the band edge and gap width to verify the FWHM decrease (Figure 7). Particle's diameter (d) and center-to-center distance between two particles (a) are adopted to descript the assembly structure. The model is based on plane wave expansion (Commercial Software Rsoft Bandsolve), and the PCs are assumed as crack-free structure. When the particles adopt more close-packed assembly structure, i.e. area contact pattern, d/a will increase, and the gap width will decrease. For example, the latex suspension drying on the substrates with high F_{ad}, the particles adopt point contact pattern (Figure 7A), where, d and a are 224 nm. d/a is 1.0, λ ranges from 512 to 545 nm, with calculated band gap width about 33 nm. In the case of the same latex suspension drying on the substrates with F_{ad} lower than 60 μN, the particles adopted area contact pattern (Figure 7B). d is 234 nm and a is 209 nm. d/a is about 1.12. λ ranges from 526 to 540 nm, with calculated band gap width about 14 nm. The calculated band gap width obviously decreases when the assembly structure becomes denser, which is in agreement with experiment results. Meantime, the low-adhesive superhydrophobic substrates benefit the formation of thick colloidal PCs, which also contribute to the narrow stopbands (Figure S7, SI).[27]

To investigate the influence of adhesive behaviors on assembly structure of colloidal PCs, we monitor the drying process of the latex particles assembled on substrates with various F_{ad} (Figure S8, SI). Different changing modes of TCL are observed: pinned TCL for high-adhesive substrate and receding TCL for low-adhesive one. Based on above phenomena, the illustration for the assembly process of the PCs on substrates with high and low adhesion is shown in Figure 8. When the latex is assembled on the high-adhesive hydrophilic or hydrophobic substrates (with $F_{ad} > 156$ μN), the latex suspension is attached to the substrate and in the Wenzel regime, forming a continuous and stable TCL.[28] Due to the pinned TCL during the whole drying process, stress production is resulted from latex particles shrinkage, which leads to the formation of cracked PCs and point contact pattern of the particles. In detail, in the beginning of the drying process, the lateral immersion capillary forces and Brownian motion of the hydrophilic latex particles induce crystalline monolayer nucleation and crystal growth on the outermost surface of liquid film.[29] The further solvent evaporation causes the particles of the whole film to shrink simultaneously, and the shrinkage is resisted by the rigid substrate (Figure S9, SI). In this case, the resistance is mainly determined by F_{ad} of the substrate. When the tensile stress generated accumulates and overlaps over the critical stress (i.e., 156 μN, evaluated by Griffith's energy balance concept[14,30]) cracks are formed in the resultant PCs. In contrast, an entirely different drying process occurs when the latex is assembled on a low-adhesive superhydrophobic substrate ($F_{ad} < 156$ μN). In this case, the suspension is in the Cassie wetting regime with a low CA hysteresis.[24] The latex suspension only touches the protruding part at the brim of the substrate, forming a discontinuous TCL. The TCL recedes continuously during the drying process in Figure 8. The TCL receding process releases the stress and contributes to the colloidal PCs with more close-packed and

17056

dx.doi.org/10.1021/ja304751k | *J. Am. Chem. Soc.* 2012, 134, 17053–17058
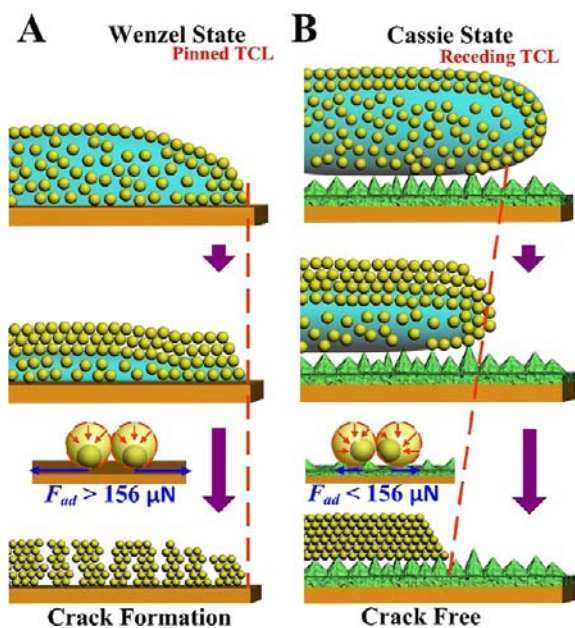
Figure 8. Schematic illustration of colloidal PCs assembled on high F_{ad} substrate (A) and low F_{ad} superhydrophobic substrate (B). The red dashed lines indicate the changing trend of the TCL during different drying conditions. The latex particles at first assemble on the surface of the suspension, and then shrink with further solvent evaporation. When the latex particles dry on a substrate with high F_{ad}, the pinned TCL and latex shrinkage causes tensile stress and crack formation. In contrast, large-scale crack-free colloidal PCs are achieved on a superhydrophobic substrate with low F_{ad} due to the timely release of tensile stress as the TCL recedes.

large-scale crack-free structure. The as-prepared PCs can be easily removed from the substrates due to the low adhesion.

Additionally, the simultaneous assembly of latex particles over the outermost layer of the spreading liquid film induces a well-ordered assembly structure,[31] and the recession of TCL ensures the formation of more close-packed PCs. All of these contribute to the narrow stopband in Figure 2B. It should be noted that well-ordered assembly structure is well confirmed by the Small-angle X-ray scattering in Figure S10 (SI). As a result, colloidal PCs with FWHMs narrower than 15 nm are achieved on the substrates with F_{ad} less than 60 μN. Importantly, the high-quality colloidal PCs can be fabricated as well when using other low-adhesive superhydrophobic substrates such as lotus leaf, which suggests the universality of the strategy (Figure S11, SI).

CONCLUSION

In summary, we have demonstrated a facile approach for achieving three-dimensional colloidal PCs with narrow stopbands on low-adhesive superhydrophobic substrates, based on the continuous recession of TCL of latex suspension during evaporation process. The FWHM of colloidal PCs can achieve 12 nm if the F_{ad} is less than 60 μN. This special property is attributed to the combined effects of large-scale crack elimination, well-ordered latex arrangement, decreased void fraction, and sufficient thickness of resultant colloidal PCs. This facile fabrication of centimeter-scale colloidal PCs with narrow stopbands is of great importance for the design and creation of advanced optical devices, especially for improving the resolution and sensitivity of PC-based sensors and detection devices.

EXPERIMENTAL SECTION

Synthesis of Latex Particles of Poly(styrene-methyl methacrylate-acrylic acid) [poly(St-MMA-AA)]. The latex particles were synthesized by one-step emulsion polymerization using our previous method,[20] which were directly used without further purification.

Preparation of Substrates with Different Adhesive Behaviors. The substrates with different adhesive behaviors were prepared by coating the polydimethylsiloxane (PDMS) modified silica nanoparticles solution (in chloroform) with different concentrations according to our previously reported method.[22] The silica nanoparticles (Aerosil R202, average particle size 14 nm) modified with poly(dimethylsiloxane) (PDMS) were made by Evonik Degussa Co. The solutions were obtained as follows, polystyrene granules (1 g, M_w 192000 g/mol, Aldrich, St Louis, MO, USA) and PDMS modified silica nanoparticles (varying from 0.2, 0.4, 0.6, 0.8, and 1.0 g) were mixed in 30 mL of chloroform and stirred for 30 min in a closed bottle. The substrates with various a F_{ad} were prepared by coating hydrophobic silica nanoparticles solution with different concentrations onto clean glass slides and basking the coated substrates at 80 °C for 1h. The substrates with different F_{ad} and water CA were obtained by coating the mixing solution with different concentrations. When the mount of silica nanoparticles in 30 mL chloroform was adopted from 0.2, 0.4, 0.6, 0.8 to 1.0 g, the F_{ad} of the resultant substrates varies from 269 ± 25 μN (CA: 98.2 ± 1.2°), 201 ± 19 μN (CA: 112.4 ± 6.1°), 171 ± 16 μN (CA: 142.1 ± 3.8°), 60 ± 7 μN (CA: 158.7 ± 1.9°) to 2 ± 1 μN (CA: 160.8 ± 3.2°). The substrate performances are shown in Figures 3 and 4. In our experiment, 5 mL beakers were treated and used as substrates.

Fabrication of PCs. The colloidal PCs were obtained by gravitational deposition method. For example, the PCs with thickness about 1800 μm (~6000 layers) and close-packed structure can be obtained when the latex suspension (1 g) with concentration of 20 wt % was added into the 5 mL treated beaker and kept at 20 °C with relative humidity of 20% for ~8 h.

Characterization. Scanning electron microscope (SEM) images of the PCs were obtained using a field-emission scanning electron microscope (JEOL-4800, Tokyo, Japan or JSM-6700F, Japan). Atomic force microscope (AFM) images were obtained using an atomic force microscope (SPI 4000). Optical microscope images were taken by system microscopy (Olympus BX51, Japan). UV−vis spectra were recorded using an Ocean Optics (Dunedin, FL, USA) HR 4000 fiber-optic UV−vis spectrometer in reflection mode, with incident light normal to the hkl = 111 crystal planes. Water static CAs and sliding angles were measured on an OCA20 machine (DataPhysics, Germany) at ambient temperature. The water F_{ad} were measured using a high-sensitivity microelectro mechanical balance system (DataPhysics DCAT 11, Germany). A water drop (3 μL) was suspended with a metal ring and controlled to squeeze the surface at a constant speed (0.005 mm·s^{-1}) and then allowed to relax. The forces were recorded continuously. The digital photographs were taken using a Nikon (Tokyo, Japan) D90 single Lens reflex camera. The dynamic process of droplet drying was captured on an OCA20 machine (DataPhysics, Germany) at ambient temperature. Small Angle X-rays (SAXS) measurements were performed at the Shanghai synchrotron radiation facility center (Shanghai, China). The X-ray wavelength was λ = 1.2400 Å. The sample-to-detector distance was LSD = 5222 mm, with an effective scattering vector q ($q = 4\pi \sin\theta/\lambda$, where 2θ is the scattering angle). The ambient temperature is about 20 °C. Polydispersity of the latex particles were obtained by dynamic light scattering (DLS) from Malvern Zetasizer Nano ZS90. The roughness (R_a) is arithmetic mean of the absolute departures of the roughness profile from the mean line, which is characterized by Surtronic 25, Taylor Hobson precision (England).

ASSOCIATED CONTENT

Ⓢ Supporting Information

Supporting Information. SEM, AFM characterization are available free of charge via the Internet at http://pubs.acs.org.

■ AUTHOR INFORMATION

Corresponding Author
ylsong@iccas.ac.cn (Y.S.); wangzhang@iccas.ac.cn (J.W.)

Author Contributions
[⊥]These authors contributed equally to this work.

Notes
The authors declare no competing financial interest.

■ REFERENCES

(1) (a) Yablonovitch, E. *Phys. Rev. Lett.* **1987**, *58*, 2059. (b) John, S. *Phys. Rev. Lett.* **1987**, *58*, 2486.
(2) Braun, P. V.; Rinne, S. A.; García-Santamaria, F. *Adv. Mater.* **2006**, *18*, 2665.
(3) Chen, J. I. L; von Freymann, G.; Choi, S. Y.; Kitaev, V.; Ozin, G. A. *Adv. Mater.* **2006**, *18*, 1915.
(4) (a) Xu, X. L.; Goponenko, A. V.; Asher, S. A. *J. Am. Chem. Soc.* **2008**, *130*, 3113. (b) Ge, J. P.; Lee, H.; He, L.; Kim, J.; Lu, Z.; Kim, H.; Goebl, J.; Kwon, S.; Yin, Y. D. *J. Am. Chem. Soc.* **2009**, *131*, 15687. (c) Gu, Z. Z.; Fujishima, A.; Sato, O. *J. Am. Chem. Soc.* **2000**, *122*, 12387. (d) Lee, K.; Asher, S. A. *J. Am. Chem. Soc.* **2000**, *122*, 9534.
(5) (a) Burgess, I. B.; Mishchenko, L.; Hatton, B. D.; Kolle, M.; Loncar, M.; Aizenberg, J. *J. Am. Chem. Soc.* **2011**, *133*, 12430.
(6) Mihi, A.; Zhang, C. J.; Braun, P. V. *Angew. Chem., Int. Ed.* **2011**, *50*, 5712.
(7) (a) Ge, J. P.; Yin, Y. D. *Angew. Chem., Int. Ed.* **2011**, *50*, 1492. (b) Zhao, Y. J.; Zhao, X. W.; Gu, Z. Z. *Adv. Funct. Mater.* **2010**, *20*, 2970. (c) Sato, O.; Kubo, S.; Gu, Z. Z. *Acc. Chem. Res.* **2009**, *42*, 1. (d) Zhang, J. H.; Yang, B. *Adv. Funct. Mater.* **2010**, *20*, 3411. (e) Sorrell, C. D.; Serpe, M. J. *Adv. Mater.* **2011**, *23*, 4088. (f) Wang, J. X.; Zhang, Y. Z.; Wang, S. T.; Song, Y. L.; Jiang, L. *Acc. Chem. Res.* **2011**, *44*, 405. (g) Kim, S. H.; Lee, S. Y.; Yang, S. M.; Yi, G. R. *NPG Asia Mater.* **2011**, *3*, 25.
(8) (a) Blanco, A.; Chomski, E.; Grabtchak, S.; Ibisate, M.; John, S.; Leonard, S. W.; López, C.; Meseguer, F.; Miguez, H.; Mondia, J. P.; Ozin, G. A.; Toader, O.; van Driel, H. M. *Nature* **2000**, *405*, 437. (b) Míguez, H.; Chomski, E.; García-Santamaría, F.; Ibisate, M.; John, S.; López, C.; Meseguer, F.; Mondia, J. P.; Ozin, G. A.; Toader, O.; van Driel, H. M. *Adv. Mater.* **2001**, *13*, 1634. (c) García-Santamaría, F.; Ibisate, M.; Rodríguez, I.; Meseguer, F.; López, C. *Adv. Mater.* **2003**, *15*, 788.
(9) Zhang, J. T.; Wang, L. L.; Luo, J.; Tikhonov, A.; Kornienko, N.; Asher, S. A. *J. Am. Chem. Soc.* **2011**, *133*, 9152.
(10) (a) Galusha, J. W.; Jorgensen, M. R.; Bartl, M. H. *Adv. Mater.* **2010**, *22*, 107. (b) Walish, J. J.; Kang, Y. J.; Mickiewicz, R. A.; Thomas, E. L. *Adv. Mater.* **2009**, *21*, 3078.
(11) (a) Hosein, I. D.; Stephanie, H. L.; Sun, Z. Q.; Chen, X.; Zhang, J. H.; Chen, Z. M.; Zhang, K; Yan, X.; Wang, Y. F.; Yu, W. Z.; Yang, B. *Langmuir* **2005**, *21*, 8987. (b) Park, S. G.; Miyake, M.; Yang, S. M.; Braun, P. V. *Adv. Mater.* **2011**, *23*, 2749.
(12) (a) Huang, X. Q.; Lai, Y.; Hang, Z. H.; Zheng, H. H.; Chan, C. T. *Nat. Mater.* **2011**, *10*, 582. (b) Hynninen, A. P.; Thijssen, H. J.; Vermolen, E. M.; Dijkstra, E.; Van Blaaderen, A. *Nat. Mater.* **2007**, *6*, 202.

(13) (a) Benabid, F.; Couny, F.; Knight, J. C.; Birks, T. A.; Russell, P. S. *Nature* **2005**, *434*, 488. (b) Kim, S. H.; Jeong, W. C.; Hwang, H.; Yang, S. M. *Angew. Chem., Int. Ed.* **2011**, *50*, 11649.
(14) (a) Singh, K. B.; Tirumkudulu, M. S. *Phys. Rev. Lett.* **2007**, *98*, 218302. (b) Zhou, J. M.; Wang, J. X.; Huang, Y.; Liu, G. M.; Wang, L. B.; Chen, S. R.; Li, X. H.; Wang, D. J.; Song, Y. L.; Jiang, L. *NPG Asia Mater.* **2012**, *4*, e21.
(15) (a) Quéré, D.; Lafuma, A.; Bico, J. *Nanotechnology* **2003**, *14*, 1109. (b) Wang, R.; Hashimoto, D.; Fujishima, A.; Chikuni, M.; Kojima, E.; Kitamura, A.; Shimohigoshi, M.; Watanabe, T. *Nature* **1997**, *388*, 431. (c) Li, Y.; Zhang, J.; Yang, B. *Nanotoday* **2010**, *5*, 117.
(16) (a) Hatton, B.; Mishchenko, L.; Davis, S.; Sandhage, K. H.; Aizenberg, J. *Proc. Natl. Acad. Sci. U.S.A.* **2010**, *107*, 10354. (b) Zheng, Z. Y.; Gao, K. Y.; Luo, Y. H.; Li, D. M.; Meng, Q. B.; Wang, Y. R.; Zhang, D. Z. *J. Am. Chem. Soc.* **2008**, *130*, 9785. (c) Wong, S.; Kitaev, V.; Ozin, G. A. *J. Am. Chem. Soc.* **2003**, *125*, 15589. (d) Shkunov, M. N.; Vardeny, Z. V.; DeLong, M. C.; Polson, R. C.; Zakhidov, A. A.; Baughman, R. H. *Adv. Funct. Mater.* **2002**, *12*, 21.
(17) (a) Sacanna, S.; Rossi, L.; Pine, D. J. *J. Am. Chem. Soc.* **2012**, *134*, 6112. (b) Wang, F.; Seo, J. H.; Ma, Z. Q.; Wang, X. D. *ACS Nano* **2012**, *6*, 2602. (c) Xu, L.; Li, H.; Jiang, X.; Wang, J. X.; Li, L.; Song, Y. L.; Jiang, L. *Macromol. Rapid Commun.* **2010**, *31*, 1422.
(18) (a) Krumpfer, J. W.; McCarthy, T. J. *J. Am. Chem. Soc.* **2011**, *133*, 5764. (b) Su, B.; Wang, S. T.; Ma, J.; Wu, Y. C.; Chen, X.; Song, Y. L.; Jiang, L. *Adv. Mater.* **2012**, *24*, 559.
(19) (a) Sun, T.; Wang, G.; Feng, L.; Liu, B.; Ma, Y.; Jiang, L.; Zhu, D. *Angew. Chem., Int. Ed.* **2004**, *43*, 357. (b) Qing, G.; Sun, T. *Adv. Mater.* **2011**, *23*, 1615.
(20) (a) Wang, J. X.; Wen, Y. Q.; Ge, H. L.; Sun, Z. W.; Zheng, Y. M.; Song, Y. L.; Jiang, L. *Macromol. Chem. Phys.* **2006**, *207*, 596. (b) Wang, J. X.; Wen, Y. Q.; Feng, X. J.; Song, Y. L.; Jiang. L. *Macromol. Rapid Commun.* **2006**, *27*, 188.
(21) (a) Gates, B.; Park, S. H.; Xia, Y. N. *Adv. Mater.* **2000**, *12*, 653. (b) Sun, F. Q.; Cai, W. P.; Li, Y.; Cao, B. Q.; Lu, F.; Duan, G. T.; Zhang, L. D. *Adv. Mater.* **2004**, *16*, 1116.
(22) Su, B.; Li, M.; Lu, Q. H. *Langmuir* **2010**, *26*, 6048.
(23) (a) Wenzel, R. N. *Ind. Eng. Chem.* **1936**, *28*, 988. (b) Sun, T. L.; Qing, G. Y.; Su, B. L.; Jiang, L. *Chem. Soc. Rev.* **2011**, *40*, 2909. (c) Sun, T. L.; Qing, G. Y. *Adv. Mater.* **2011**, *23*, H57. (c) Liu, M. J.; Wang, S. T.; Wei, Z. X.; Song, Y. L.; Jiang, L. *Adv. Mater.* **2009**, *21*, 665. (d) Liu, M. J.; Jiang, L. *Adv. Funct. Mater.* **2010**, *20*, 3753.
(24) (a) Cassie, A. B. D.; Baxter, S. *Trans. Faraday. Soc.* **1944**, *40*, 546. (b) Lafuma, A.; Quéré, D. *Nat. Mater.* **2003**, *2*, 457. (c) Yao, X.; Chen, Q. W.; Xu, L.; Li, Q. K.; Song, Y. L.; Gao, X. F.; Quéré, D.; Jiang, L. *Adv. Funct. Mater.* **2010**, *20*, 656. (d) Huang, Y.; Liu, M. J.; Wang, J. X.; Zhou, J. M.; Wang, L. B.; Song, Y. L.; Jiang, L. *Adv. Funct. Mater.* **2011**, *21*, 4436.
(25) (a) Richel, A.; Johnson, N. P.; McComb, D. W. *Appl. Phys. Lett.* **2000**, *76*, 1816. (b) Busch, K.; John, S. *Phys. Rev. E.* **1998**, *58*, 3896.
(26) Rundquist, P. A.; Photinos, P.; Jagannathan, S.; Asher, S. A. *J. Chem. Phys.* **1989**, *91*, 4932.
(27) (a) Jiang, P.; Bertone, J. F.; Hwang, K. S.; Colvin, V. L. *Chem. Mater.* **1999**, *11*, 2132. (b) Bertone, J. F.; Jiang, P.; Hwang, K. S.; Mittleman, D. M.; Colvin, V. L. *Phys. Rev. Lett.* **1999**, *83*, 300.
(28) Deegan, R. D.; Bakajin, O.; Dupont, T. F.; Huber, G.; Nagel, S. R.; Witten, T. A. *Nature* **1997**, *389*, 827.
(29) Denkov, N. D.; Velev, O. D.; Kralchevsky, P. A.; Ivanov, I. B.; Yoshimura, H.; Nagayama, K. *Nature* **1993**, *361*, 26.
(30) (a) Tirumkululu, M. S.; Russel, W. B. *Langmuir* **2005**, *21*, 4938. (b) Jagota, A.; Hui, C. Y. *Mech. Mater.* **1991**, *11*, 221.
(31) Rastogi, V.; Melle, S.; Calderón, O. G.; García, A. A.; Marquez, M.; Velev, O. D. *Adv. Mater.* **2008**, *20*, 4263.